Polymer Chemistry

PAPER

View Article Online
View Journal | View Issue

Cite this: *Polym. Chem.*, 2014, **5**, 6190

Polythiophenes with vinylene linked *ortho*, *meta* and *para*-carborane sidechains†

Jonathan Marshall,[a] Jake Hooton,[a] Yang Han,[a] Adam Creamer,[a] Raja Shahid Ashraf,[a] Yoann Porte,[b] Thomas D. Anthopoulos,[c] Paul N. Stavrinou,[c] Martyn A. McLachlan,[b] Hugo Bronstein,[d] Peter Beavis[e] and Martin Heeney*[a]

Received 31st May 2014,
Accepted 8th July 2014

DOI: 10.1039/c4py00767k

www.rsc.org/polymers

We report the synthesis of a series of novel polythiophenes with vinylene linked pendant carborane sidechains. Polymers containing *ortho*, *meta* and *para* substituted carborane linked *via* a *cis* or *trans* double bond are reported. The inclusion of carborane sidechains is demonstrated to afford soluble polymers without the presence of any additional alkyl groups. The choice of carborane and double bond isomer is shown to influence the optoelectronic, photovoltaic and charge-transporting properties of the polymer. In particular the incorporation of *ortho*-carborane was shown to have a pronounced electron withdrawing effect resulting in a substantial increase in polymer ionisation potential. Field effect transistors and solar cells devices fabricated from the various isomers showed significant differences in performance.

Introduction

Polythiophenes have been extensively studied as organic semiconductors suitable for use as the active layer components of both organic photovoltaic (OPV)[1–3] and organic field-effect transistor (OFET)[4,5] devices. For these applications it is important that the polymer can be solution processed into thin, homogeneous films.[6–8] Most polythiophenes (and the vast majority of conjugated polymers) achieve the required processability through the incorporation of long alkyl chains, both linear and branched, onto the polymer backbone. In addition to promoting solubility, the sidechains influence thermal behaviour and intermolecular interactions of the polymers.[9,10] As such, the choice of sidechain can have an important role in device performance. Recently it has been demonstrated that the use of conjugated sidechains – solubilising units that are linked to the conjugated backbone *via* a sp or sp^2 hybridised group – is an effective way of tuning both processability and the electronic structure of the polymer backbone. The resultant polymers have been termed as two-dimensionally conjugated structures, in which the choice of conjugated sidechain can modify optical absorption, energy levels, solubility and aggregation properties, all of which can be tailored to improve optoelectronic device performance.[11]

For example, research undertaken by Liu, Li and co-workers demonstrated that polymeric absorption spectrum could be broadened by replacing an hexyl sidechain with an hexy-1-enyl unit, facilitating the improved absorption of incident photons and therefore an improvement in photovoltaic power conversion efficiency.[12] They further noted that, in comparison to main chain polythiophene vinylene polymers, both the HOMO and LUMO energy levels were lowered, leading to a polymer with increased oxidative stability and an open-circuit voltage (V_{OC}) approximately 0.2 eV greater than poly(3-hexyl)thiophene (P3HT) upon employment in a photovoltaic device. Further research by the same group showed that by expanding the series to include a range of electron withdrawing and donating conjugated pendant groups, it was possible to effectively modulate polymer energetics and charge-transporting characteristics, tailoring them for use in specific optoelectronic applications.[13,14] Additionally, consideration of the structure of – and spacing between – pendant groups was shown to offer a means of improving backbone planarity and material crystallinity, further improving device performance.[15–17]

We were interested to investigate the potential of carboranes as conjugated solubilising groups. Carboranes are exceptionally stable polyhedral clusters of carbon and boron that exhibit an unusual three dimensionally delocalised electronic structure (Fig. 1).[18] We anticipated that the incorporation of carborane, with its regular icosahedral shape, may promote polymer solubility, whilst the conjugation of the inductively

[a]*Department of Chemistry and Centre for Plastic Electronics, Imperial College London, London, SW7 2AZ, UK. E-mail: m.heeney@imperial.ac.uk*
[b]*Department of Materials and Centre for Plastic Electronics, Imperial College London, London, SW7 2AZ, UK*
[c]*Department of Physics and Centre for Plastic Electronics, Imperial College London, London, SW7 2AZ, UK*
[d]*Department of Chemistry, University College London, London, WC1H 0AJ, UK*
[e]*AWE, Aldermaston, Reading, RG7 4PR, UK*

†Electronic supplementary information (ESI) available: ^{1}H NMR of novel compounds, DFT optimised geometries, DFT visualised frontier orbitals, TGA traces, OFET output and transfer curves. See DOI: 10.1039/c4py00767k

Fig. 1 Structures of (left–right): *ortho*-carborane, *meta*-carborane and *para*-carborane. Unlabelled vertices represent BH units. Protons omitted for clarity.

electron-withdrawing cage to the thiophene backbone *via* an electronically communicative ethylene linker may allow manipulation of the conjugated backbone properties.

Some research has been carried out into the effects of pendant carborane cages on the properties of conjugated polymers, although to date the carboranes have either been connected *via* an alkyl chain linker, or directly fused to the conjugated backbone.[19–30] Hence polymers with pendant carborane units have been demonstrated to possess high stability in thermally-annealed films, a feature anticipated to be inherently useful for functional conjugated polymers whose applications are realised in the solid state.[18] Furthermore, polyfluorene derivatives incorporating silyl substituted *ortho*-carboranes, connected *via* an alkyl chain linker, have demonstrated enhanced solubility and suppressed aggregation (which in this instance was desirable), suggesting that the carborane cage may be effective at promoting polymer solubility.[31] In addition, the inclusion of carborane led to a raise in the glass transition temperature (T_g) and enhanced oxidative and thermal stability. Other examples show sensing properties, in which their photoluminescence emission spectra are bathochromically shifted upon exposure to solvent vapours of increasing polarity,[24] and some carborane containing small molecules have been shown to exhibit interesting non-linear optical properties.[32]

However the previous work on pendant carborane groups has focussed on *ortho*-carborane only, offering significant scope for further research. Carborane exists in three isomers – *ortho*, *meta* and *para* – distinguished by the spacing of carbon atoms around the cage and the different properties that result from varying polarities between the isomers (Fig. 1). The spacing of the relatively electron-rich carbon atoms also determines the electron withdrawing effect of the isomers, which decreases from *ortho* > *meta* > *para*. By connecting all three carborane isomers to the polymer backbone by a conjugated yet flexible ethylene linker group, we were interested to investigate the influence of the carborane regiochemistry, as well as the relative stereochemistry of the ethylene unit, *i.e. cis* or *trans*, on the polymer properties. Here we report, for the first time, a systematic study of the effects of the incorporation of all three carborane isomers on the properties of a polythiophene backbone. We report the fundamental optoelectronic properties, as well as the influence on field effect transistor and organic solar cell device performance.

Experimental

Carborane isomers were purchased from Katchem and sublimed before use. All other reagents were purchased from Sigma-Aldrich, VWR, Alfa Aesar or Apollo scientific and were used without further purification. Dry solvents for anhydrous reactions were purchased from Sigma Aldrich. All reactions were carried out under an inert Argon atmosphere unless otherwise stated. ^{1}H $\{^{11}$B$\}$ NMR, ^{11}B $\{^1$H$\}$ NMR and ^{13}C NMR spectra were recorded on a BRUKER 400 spectrometer in $CDCl_3$ solution at 298 K unless otherwise stated. Proton NMRs were recorded after boron decoupling and boron NMRs were recorded after proton decoupling. Number-average (M_n) and weight-average (M_w) molecular weights were determined with an Agilent Technologies 1200 series GPC in chlorobenzene at 80 °C using two PL mixed B columns in series, and calibrated against narrow polydispersity polystyrene standards. UV-Vis absorption spectra were recorded on a UV-1601 Shimadzu UV-Vis spectrometer. Column chromatography was carried out on normal-phase and reverse-phase (RP18) silica gel (VWR) on a Biotage Isolera One. Microwave reactions were performed in a Biotage initiator v.2.3. Photo Electron Spectroscopy in Air (PESA) measurements were recorded using a Riken Keiki AC-2 PESA spectrometer with a power setting of 5 nW and a power number of 0.5. Differential scanning calorimetry (DSC) measurements were made using a TA instruments DSC TZero Q20 instrument and analysed using TA universal analysis software. Thermal Gravimetric analysis measurements were recorded using a Perkin Elmer Pyris 1 TGA. X-Ray Diffraction (XRD) measurements were carried out using a Panalytical X'pert-pro MRD diffractometer fitted with a nickel-filtered Cu Kα 1 beam and an X'celerator detector using a current of 40 mA and an accelerating voltage of 40 kV.

1-Formyl-*ortho*-carborane

Freshly sublimed *ortho*-carborane (7.5 g, 52 mmol) was dissolved in anhydrous diethyl ether (150 mL) and cooled to −78 °C. To this solution was added *n*-BuLi (36 mL of 1.6 M in hexanes, 57.6 mmol) slowly, before the mixture was stirred at −78 °C for 2.5 h. Anhydrous methyl formate (12.5 g, 208 mmol) was added and stirring continued at −78 °C for 2 h. The reaction was quenched by the addition of dilute hydrochloric acid (4%, 100 mL) and allowed to warm to room temperature overnight. The reaction mixture was poured into water and extracted with diethyl ether. The organic layers were combined and washed with saturated sodium hydrogen carbonate solution, water and brine before being dried over magnesium sulphate and concentrated under reduced pressure. Purification by column chromatography (eluent: chloroform) and recrystallisation from hexane yielded the product as a white crystalline solid (5.9 g, 34 mmol, 66%). Mp = 204–207 °C (lit[33] = 208–209 °C). ^{1}H NMR (400 MHz, $CDCl_3$): δ 9.28 (s, 1H), 4.06 (s, 1H), 3.04–1.63 (m, 10H); ^{13}C NMR (100 MHz, $CDCl_3$): δ 184.14, 54.14; ^{11}B $\{^1$H$\}$ NMR (400 MHz, $CDCl_3$) δ 1.68, −8.56, −12.14, −12.68, −13.65. MS (EI): m/z = 172.25 (M^+).

1-Formyl-*meta*-carborane

Freshly sublimed *meta*-carborane (6.0 g, 41.7 mmol) was dissolved in anhydrous diethyl ether (100 mL) and cooled to −78 °C. To this solution was added *n*-BuLi (28.8 mL of 1.6 M

in hexanes, 46.1 mmol) slowly before the reaction mixture was stirred at −78 °C for 2.5 h. Anhydrous methyl formate (9 g, 149 mmol) was added and stirring continued at −78 °C for 2 h. The reaction mixture was quenched by the addition of dilute hydrochloric acid (4%, 75 mL) and allowed to warm to room temperature overnight. The reaction mixture was poured into water and extracted with diethyl ether. The organic layers were combined and washed with saturated sodium hydrogen carbonate solution, water and brine before being dried over magnesium sulphate and concentrated under reduced pressure. Purification by column chromatography (eluent: chloroform) and recrystallisation from hexane yielded the product as a white crystalline solid (3.98 g, 23.1 mmol, 55%). Mp = 205–209 °C (lit[33] = 213–214 °C). ^{1}H NMR (400 MHz, $CDCl_3$): δ 9.04 (s, 1H), 3.08 (s, 1H), 2.91–2.20 (m, 10 H); ^{13}C NMR (100 MHz, $CDCl_3$): δ 185.48, 55.53; ^{11}B $\{^{1}H\}$ NMR (400 MHz, $CDCl_3$) −6.29, −10.29, −12.63, −16.32. MS (EI): m/z = 172.29 (M^+).

1-Formyl-*para*-carborane

Freshly sublimed *para*-carborane (1.56 g, 10.8 mmol) was dissolved in anhydrous diethyl ether (10 mL) and cooled to −78 °C. To this solution was added *n*-BuLi (7.4 mL of 1.6 M in hexanes, 11.9 mmol) slowly before the reaction mixture was stirred at −78 °C for 2.5 h. Anhydrous methyl formate (2.7 g, 44 mmol) was added and stirring continued at −78 °C for 2 h. The reaction mixture was quenched by the addition of dilute hydrochloric acid (4%, 15 mL) and allowed to warm to room temperature overnight. The reaction mixture was poured into water and extracted with diethyl ether. The organic layers were combined and washed with saturated sodium hydrogen carbonate solution, water and brine before being dried over magnesium sulphate and concentrated under reduced pressure. Purification by column chromatography (eluent: chloroform) and recrystallisation from hexane yielded the product as a white crystalline solid (1.52 g, 8.8 mmol, 82%). Mp = 202–207 °C (lit[33] = 208.5–210 °C). ^{1}H NMR (400 MHz, $CDCl_3$): δ 8.75 ppm (s, 1H), 2.89 ppm (s, 1H), 2.34 ppm (s, 5H), 2.29 ppm (s, 5H); ^{13}C NMR (100 MHz, $CDCl_3$): δ 185.78, 63.24; ^{11}B $\{^{1}H\}$ NMR (400 MHz, $CDCl_3$) −14.56, −14.76. MS (EI): m/z = 172.20 (M^+).

3-(Bromomethyl)-2,5-dibromothiophene

2,5-Dibromo-3-methylthiophene (25 g, 98 mmol) was dissolved in carbon tetrachloride (200 mL) before *N*-bromosuccinimide (17.4 g, 98 mmol) and benzoyl peroxide (20 mg, 0.1 mmol) were added. The resulting mixture was shielded from light and heated to reflux for 3 h. After cooling to room temperature the reaction was filtered. The filtrate was washed with water, saturated sodium hydrogen carbonate solution and brine, dried ($MgSO_4$), filtered and concentrated under reduced pressure. The resulting oil was distilled (115 °C at 0.5 mbar) to afford the product as a colourless oil (23.2 g, 69.3 mmol, 71%). ^{1}H NMR (400 MHz, $CDCl_3$): δ 7.00 (s, 1H), 4.66 (s, 2H); ^{13}C NMR (100 MHz, $CDCl_3$): δ 141.9, 134.55, 115.52, 112.13, 20.94. MS (EI, GC-MS): m/z = 334.80 (M^+).

3-(Methyl-2,5-dibromothienyl)-triphenylphosphonium bromide

3-(Bromomethyl)-2,5-dibromothiophene (23.15 g, 69 mmol) and triphenylphosphine (36.4 g, 138 mmol) were dissolved in anhydrous hexane (1000 mL) and stirred at 70 °C for 6 days. After cooling to room temperature the mixture was filtered and the precipitate was washed thoroughly with hexanes to yield a white solid (28.2 g, 47.2 mmol, 68%). Mp > 300 °C. ^{1}H NMR (400 MHz, $CDCl_3$): δ 7.85–7.65 (m, 15H), 6.94 (s, 1H), 5.62 (d, J = 13.9 Hz, 2H); ^{13}C NMR (100 MHz, $CDCl_3$): δ 135.3, 134.3, 131.9, 130.3, 128.0, 117.8, 117.0, 115.0, 112.4; ^{31}P NMR (400 MHz, $CDCl_3$): δ 21.67. MS (EI) m/z = 597.13 (M^+).

3-Vinyl-*o*-carborane-2,5-dibromothiophene (*cis* (a) and *trans* (b))

3-(Methyl-2,5-dibromothienyl)-triphenylphosphonium bromide (3.2 g, 5.3 mmol) was suspended in anhydrous THF (300 mL) before potassium *t*-butoxide (5.8 mL of 1.0 M in THF, 5.8 mmol) was added dropwise. The resulting mixture was stirred at room temperature for 1 h before a solution of 1-formyl-*ortho*-carborane (1.0 g (5.8 mmol) in anhydrous THF (10 mL)) was added, and the resulting mixture heated to reflux for 3 h. The solution was allowed to cool to room temperature and stirred for 16 h before being quenched with dilute hydrochloric acid (10%, 100 mL). The mixture was washed with water and brine before the organic layers were dried over magnesium sulphate and concentrated under reduced pressure. Purification by column chromatography (eluent: hexane) yielded the *cis*-isomer as a white solid (930.0 mg, 2.3 mmol, 43%) and the *trans* isomer as a white solid (130.5 mg, 0.32 mmol, 6%). Excess *cis*-product (400 mg, 0.98 mmol) could be converted quantitatively to the *trans* isomer by UV irradiation (365 nm, 100 W) for 3 hours in chloroform (5 mL) in a quartz cuvette, with final purification by column chromatography on silica (eluent: hexane). (**a**) Mp = 52–55 °C. ^{1}H NMR (400 MHz, $CDCl_3$): δ 6.80 (s, 1H), 6.22 (d, J = 12.2 Hz 1H), 5.93 (d, J = 12.2 Hz 1H), 3.59 (s, 1H), 2.38–2.10 (m, 10H); ^{13}C NMR (100 MHz, $CDCl_3$): δ 135.12, 130.79, 129.62, 127.52, 112.28, 110.66, 63.25, 58.82; ^{11}B $\{^{1}H\}$ NMR (400 MHz, $CDCl_3$) −2.06, −3.78, −9.16, −11.13, −12.96. MS (EI, GC-MS): m/z = 410.44 (M^+). Elemental analysis: calculated for $C_8H_{14}B_{10}Br_2S_2$, C, 23.43; H, 3.44; found: C 23.51; H 3.31. (**b**) Mp = 116–120 °C. ^{1}H NMR (400 MHz, $CDCl_3$): δ 6.98 (s, 1H), 6.76 (d, J = 15.7 Hz, 1H), 6.12 (d, J = 15.7 Hz, 1H), 3.70 (s, 1H), 2.47–2.23 (m, 10H); ^{13}C NMR (100 MHz, $CDCl_3$): δ 135.99, 128.81, 126.94, 125.00, 113.81, 112.85, 73.38, 60.82; ^{11}B $\{^{1}H\}$ NMR (400 MHz, $CDCl_3$) −1.84, −4.75, −9.06, −11.00, −11.79, −12.80. MS (EI, GC-MS): m/z = 410.37 (M^+). Elemental analysis: calculated for $C_8H_{14}B_{10}Br_2S_2$, C, 23.43; H, 3.44; found: C 23.54; H 3.34.

3-Vinyl-*m*-carborane-2,5-dibromothiophene (*cis* (a) and *trans* (b))

3-(Methyl-2,5-dibromothienyl)-triphenylphosphonium bromide (3.0 g, 5.0 mmol) was suspended in anhydrous THF (300 mL) before potassium *t*-butoxide (5.0 mL of 1.0 M in THF, 5.0 mmol) was added dropwise. The resulting mixture was stirred at room temperature for 1 h before a solution of

1-formyl-*meta*-carborane (760 mg in anhydrous THF (10 mL)) was added, and the mixture was heated at reflux for 3 hours. The solution was allowed to cool to room temperature and stirred for 16 h before being quenched with dilute hydrochloric acid (10%, 100 mL). The mixture was washed with water and brine before the organic layers were dried over magnesium sulphate and concentrated under reduced pressure. Purification by reverse-phase column chromatography on RP18 (eluent: acetonitrile) yielded the *cis*-isomer as a white solid (1.10 g, 2.7 mmol, 55%) and the *trans* isomer as a white solid (975 mg, 2.37 mmol, 43%). (**a**) Mp = 49–54 °C. ^{1}H NMR (400 MHz, $CDCl_3$): δ 6.79 (s, 1H), 6.03 (d, J = 12.0 Hz, 2H), 5.73 (d, J = 12.0 Hz, 1H), 3.33 (s, 1H), 2.66–2.06 (m, 10H); ^{13}C NMR (100 MHz, $CDCl_3$): δ 131.67, 131.24, 125.99, 110.77; ^{11}B $\{^1$H$\}$ NMR (400 MHz, $CDCl_3$) δ −6.31, −10.31, −13.44, −14.89, −16. 84. MS (EI, GC-MS): m/z = 410.31 (M^+). Elemental analysis: calculated for $C_8H_{14}B_{10}Br_2S_2$, C, 23.43; H, 3.44; found: C 23.52; H 3.42. (**b**) Mp = 129–134 °C. ^{1}H NMR (400 MHz, $CDCl_3$): δ 6.95 (s, 1H), 6.53 (d, J = 15.6 Hz, 2H), 5.98 (d, J = 15.6 Hz, 2H), 3.29 (s, 1H), 2.89–2.13 (m, 10H); ^{13}C NMR (100 MHz, $CDCl_3$): δ 136.90, 127.40, 127.13, 126.00, 112.27, 112.07, 61.69, 58.77; ^{11}B $\{^1$H$\}$ NMR (400 MHz, $CDCl_3$) −5.50, −8.08, −10.38, −12.77. MS (EI, GC-MS): m/z = 410.41 (M^+). Elemental analysis: calculated for $C_8H_{14}B_{10}Br_2S_2$, C, 23.43; H, 3.44; found: C 23.54; H 3.55.

3-Vinyl-*p*-carborane-2,5-dibromothiophene (*cis* (a) and *trans* (b))

3-(Methyl-2,5-dibromothienyl)-triphenylphosphonium bromide (4.6 g, 7.7 mmol) was suspended in anhydrous THF (300 mL) before potassium *t*-butoxide (7.7 mL of 1.0 M in THF, 7.7 mmol) was added dropwise. The resulting mixture was stirred at room temperature for 1 h. To this was added a solution of 1-formyl-*para*-carborane (1.2 g in anhydrous THF (10 mL)) before the mixture was heated at reflux for 3 h. The solution was allowed to cool to room temperature and stirred for 16 hours before being quenched with dilute hydrochloric acid (10%, 140 mL). The mixture was washed with water and brine before the organic layers were dried over magnesium sulphate and concentrated under reduced pressure. Purification by reverse-phase column chromatography on RP18 (eluent: acetonitrile) yielded the *cis*-isomer as a white solid (940 mg, 2.3 mmol, 33%) and the *trans* isomer as a white solid (600 mg, 1.5 mmol, 21%). (**a**) Mp = 51–55 °C. ^{1}H NMR (400 MHz, $CDCl_3$): δ 6.71 (s, 1H), 5.83 (d, J = 12.0 Hz, 1H), 5.45 (d, J = 12.0 Hz, 1H), 2.90–1.55 (m, 11H); ^{13}C NMR (100 MHz, $CDCl_3$): δ 136.17, 132.78, 131.75, 124.69, 110.56, 110.46, 60.71; ^{11}B $\{^1$H$\}$ NMR (400 MHz, $CDCl_3$) −12.32, −15.04. MS (EI, GC-MS): m/z = 410.47 (M^+). Elemental analysis: calculated for $C_8H_{14}B_{10}Br_2S_2$, C, 23.43; H, 3.44; found: C 23.34; H 3.34. (**b**) Mp = 145–149 °C. ^{1}H NMR (400 MHz, $CDCl_3$): δ 6.86 (s, 1H), 6.27 (d, J = 16.0 Hz 2H), 5.71 (d, J = 16.0 Hz 2H), 3.01–1.61 (m, 11H); ^{13}C NMR (100 MHz, $CDCl_3$): δ 136.95, 129.33, 127.11, 124.63, 112.10, 111.86, 59.05; ^{11}B $\{^1$H$\}$ NMR (400 MHz, $CDCl_3$) −12.64, −15.20. MS (EI, GC-MS): m/z = 410.42 (M^+). Elemental analysis: calculated for $C_8H_{14}B_{10}Br_2S_2$, C, 23.43; H, 3.44; found: C 23.36; H 3.34.

Polymerisation procedure

A clean, dry microwave vial was charged with 2,5-bis-(trimethylstannyl)thiophene (300 mg, 0.73 mmol), 1.0 eq. of dibrominated monomer, 2 mol% tris(dibenzylideneacetone) dipalladium (0) and 8 mol% of tri(*o*-tolyl) phosphine. The vial was sealed before anhydrous chlorobenzene (1.5 mL) was added. The resulting solution was degassed with argon for 45 minutes before heating in the microwave reactor: 100 °C for 5 minutes, 140 °C for 5 minutes, 180 °C for 5 minutes and finally 200 °C for 30 minutes. The mixture was allowed to cool to room temperature before the crude polymer was precipitated in acidified methanol and further purified by Soxhlet extractions with methanol (24 hours), acetone (24 hours), *n*-hexane (24 hours) chloroform (24 hours) and chlorobenzene (24 hours). The chlorobenzene solution was stirred with an aqueous solution of sodium diethyldithiocarbamate (*ca*. 0.25 g in 50 mL) for 3 h at 50 °C with vigorous stirring. The organic phase was separated from the aqueous phase and washed several times with water. The polymer solution was concentrated under reduced pressure and precipitated into methanol. The resulting precipitate was washed with acetone and dried under high vacuum for 24 hours.

ortho*/*cis: Dark-red solid (127 mg, 0.38 mmol, 52%) M_n = 17 kg mol^{-1}, M_w = 22 kg mol^{-1}, Đ = 1.3. Elemental analysis: calculated for $C_{14}H_{16}B_{10}S_2$, C, 43.35; H, 4.85; found: C 43.44; H 4.76.

ortho*/*trans: Dark-red solid (144 mg, 0.42 mmol, 59%) M_n = 15 kg mol^{-1}, M_w = 21 kg mol^{-1}, Đ = 1.4. Elemental analysis: calculated for $C_{14}H_{16}B_{10}S_2$, C, 43.35; H, 4.85; found: C 43.24; H 4.89.

meta*/*cis: Dark-red solid (155 mg, 0.44 mmol, 60%) M_n = 18 kg mol^{-1}, M_w = 27 kg mol^{-1}, Đ = 1.5. Elemental analysis: calculated for $C_{14}H_{16}B_{10}S_2$, C, 43.35; H, 4.85; found: C 43.54; H 4.79.

meta*/*trans: Dark-red solid (98 mg, 0.29 mmol, 40%) M_n = 12 kg mol^{-1}, M_w = 19 kg mol^{-1}, Đ = 1.6. Elemental analysis: calculated for $C_{14}H_{16}B_{10}S_2$, C, 43.35; H, 4.85; found: C 43.49; H 4.92.

para*/*cis: Dark-red solid (131 mg, 0.39 mmol, 54%) M_n = 17 kg mol^{-1}, M_w = 20 kg mol^{-1}, Đ = 1.2. Elemental analysis: calculated for $C_{14}H_{16}B_{10}S_2$, C, 43.35; H, 4.85; found: C 42.51; H 3.39.

para*/*trans: Dark-red solid (65 mg, 0.19 mmol, 27%) M_n = 12 kg mol^{-1}, M_w = 20 kg mol^{-1}, Đ = 1.7. Elemental analysis: calculated for $C_{14}H_{16}B_{10}S_2$, C, 43.35; H, 4.85; found: C 43.30; H 4.76.

Transistor fabrication details

All film preparation steps were carried out under inert atmosphere. Thin films (*ca*. 20 nm) of the polymers were spun-cast from chlorobenzene solutions (5 m mL^{-1}) on glass substrates with lithographically patterned and pentafluorobenzenethiol-treated Au source/drain electrodes before a thermal annealing at 160 °C for 10 min. A perfluorinated polymer (CYTOP CTL-809M from Asahi Glass) was used as gate dielectric and

applied *via* spin coating for 60 s at 2000 rpm and cured at 100 °C for 90 min. 50 nm aluminium was evaporated on top of the dielectric as a gate electrode to complete the device.

Organic photovoltaic device fabrication

A conventional device configuration was employed: ITO/PEDOT : PSS/polymer : $PC_{71}BM$/Ca/Al. The precoated ITO glass substrates were cleaned by sonicating in water, acetone and isopropanol successively, followed by drying and oxygen plasma treatment. A 35 nm layer of PEDOT : PSS was spin-coated onto the plasma-treated ITO substrate and baked at 150 °C for 20 minutes. The active layer consisting of a 1 : 2 in weight ratio blend of polymer and $PC_{71}BM$ dissolved in 1,2-dichlorobenzene (DCB) at 10 mg ml^{-1} of polymer was spin-coated on the PEDOT : PSS layer and then Ca (25 nm)/Al (100 nm) cathode was finally deposited by thermal evaporation under high vacuum (10^{-6} mbar) through a shadow mask. The pixel size, defined by the spatial overlap of the ITO anode and Ca/Al cathode, was 0.045 cm^2. Current density–voltage (*J–V*) characteristics were measured using a xenon lamp at AM1.5 solar illumination (Oriel Instruments) calibrated to a silicon reference cell with a Keithley 2400 source meter, correcting for spectral mismatch.

Results and discussion

Synthesis

The synthesis of *ortho*/*cis* and *ortho*/*trans* monomers is shown in Scheme 1 and follows a Wittig strategy to attach carborane to the thiophene monomer *via* a double bond.[34] The thiophene containing phosphonium salt was synthesised by radical bromination of 3-methyl-2,5-dibromothiophene (**1**) to 3-bromomethyl-2,5-dibromothiophene (**2**) in 71% yield, followed by reaction with triphenylphosphine to afford the phosphonium salt (**3**) in 68% yield. Subsequent treatment of (**3**) with potassium *tert*-butoxide afforded the ylide which was reacted directly with 1-formyl-*ortho*-carborane (**5**) to afford the desired product as a mixture of *cis* (**6**) and *trans* (**7**) isomers in 49% yield. The *cis* and *trans* isomers could be readily separated by column chromatography to afford **6** in 6% yield and **7** in 43% yield ($E : Z = 1 : 7$). In order to have sufficient *trans* isomer for the subsequent polymerisation, some of the *cis* product was quantitatively converted to the *trans* isomer by irradiation with UV light (365 nm, 100 W). The overall synthetic scheme was repeated for *meta* and *para* isomers of carborane, affording the series of monomers investigated in this work (Fig. 2).

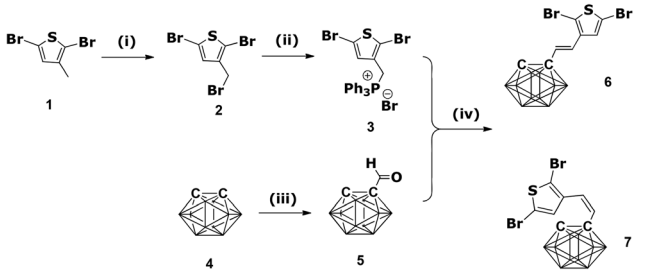

Scheme 1 Synthesis of *ortho*/*cis* and *ortho*/*trans* monomers. (i) NBS, benzoyl peroxide, 71%. (ii) Triphenylphosphine, hexane, 68%. (iii) *n*-BuLi then methyl formate, 66%. (iv) Potassium *tert*-butoxide, THF, 6% (**6**), 43% (**7**).

In all cases the *cis* isomer predominated, although the *cis*/*trans* ratio was much lower in the case of the *meta* (1.25 : 1) and *para* (1.5 : 1) substituted carboranes, precluding the need for UV-induced isomerisation for these isomers. The significant differences in product ratio for the three carborane isomers are likely due to a combination of steric and electronic effects.

Stille polymerisation with 2,5-bis(trimethylstannyl)thiophene was performed under microwave-assisted coupling conditions (Scheme 2).[35] The crude polymers were precipitated into acidified methanol and purified by sequential Soxhlet extractions in methanol, acetone, *n*-hexane, chloroform and chlorobenzene, the latter of which was retained. Palladium salts were removed by treatment with sodium diethyldithiocarbamate and subsequent aqueous extraction.[36] The yields of the isolated soluble fractions were in the range of 40–60% for all polymers (Table 1) except *para*/*trans*, which was substantially lower at 27%, owing to reduced solubility in refluxing chlorobenzene.

The molecular weights of all six polymers were measured by GPC in hot (80 °C) chlorobenzene and reported as their polystyrene equivalents (Table 1). In all instances a soluble polymer was obtained, suggesting that the inclusion of the

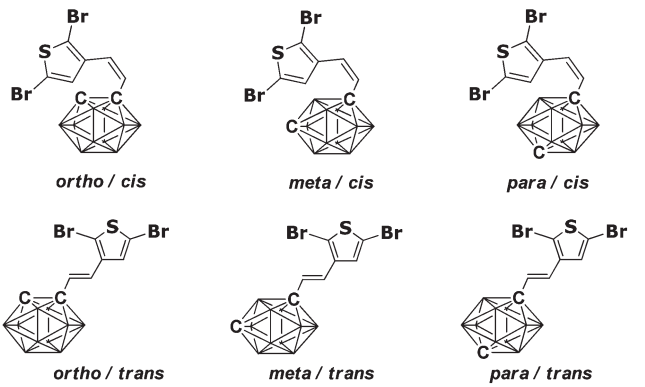

Fig. 2 Structures of the six monomers investigated in this work. Non-labelled cage-vertices represent BH units, protons omitted for clarity.

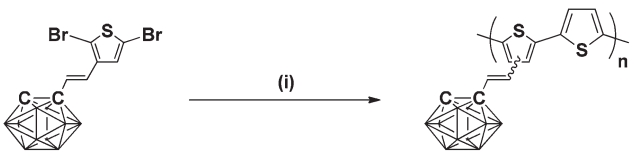

Scheme 2 Synthesis of *ortho*/*trans* polymer. (i) 2,5-bis(trimethylstannyl)thiophene, $Pd_2(dba)_3$, P(*o*-tol)$_3$, μw, 59%.

Table 1 Polymer molecular weights

Polymer	Yield	M_n [a] (kg mol^{-1})	M_w [a] (kg mol^{-1})	D_p [b]
ortho/*cis*	52%	17	22	51
ortho/*trans*	59%	15	21	45
meta/*cis*	60%	18	27	54
meta/*trans*	40%	12	19	36
para/*cis*	54%	17	20	51
para/*trans*	27%	12	20	36

[a] Determined by GPC and reported as their polystyrene equivalents. [b] Based on M_n.

Table 2 Optical properties

Polymer	λ_{max} Sol.[a] (nm)	λ_{max} film[b] (nm)	λ_{max} Ann. film[b,c] (nm)
ortho/*cis*	485	534	529
ortho/*trans*	470	533	527
meta/*cis*	492	525	519
meta/*trans*	477	535	524
para/*cis*	494	534	530
para/*trans*	495	524	518

[a] Measured in dilute chlorobenzene solution. [b] Spin-coated from 5 mg mL^{-1} chlorobenzene solution. [c] Annealed at 160 °C.

vinyl carborane pendant group is an effective means of solubilising the polythiophenes. The *cis* polymers were all substantially more soluble than their *trans* counterparts, potentially due to greater pendant group flexibility that results from reduced *p*-orbital overlap across the double bond. Although there was some variance in molecular weights across the series, the degrees of polymerisation (D_p) estimated from GPC were sufficiently high to enable a meaningful comparison to both existing materials and to each other.

For all polymers, attempts to assess backbone regioregularity by ^{1}H NMR analysis were problematic. Only broad spectra were obtained, which were ascribed to the propensity for the polymers to aggregate in solution, as well as the restricted segmental mobility for polymeric materials. From the synthetic route utilised it was expected that regiorandom polymers would be synthesised, however previous work has noted that there can be a slight preference for oxidative insertion of the palladium catalyst into either the 2 or 5 position, potentially leading to some regioregularity of the sidechain.[37,38]

Optical properties

UV-vis absorption spectra of the polymers were recorded in dilute chlorobenzene solutions and from spin-coated thin films. In solution, it was observed that both the carborane isomer and vinyl bond stereochemistry had an influence on absorption maximum and peak shape (Fig. 3). Optical data is summarised in Table 2. A number of trends are apparent, firstly in all instances (*cis* and *trans* isomers), polymers containing *ortho*-carborane exhibit the most blue-shifted λ_{max}, followed by the *meta* isomers, with the *para* isomers being the most red-shifted. Secondly, for the *ortho* and *meta*-carboranes, the *trans* isomers are consistently more blue-shifted than the *cis* isomers. For *para*-carborane, both *cis* and *trans* isomers have a similar absorption maxima. The trends in solution seem to track with the electron-withdrawing strength of the carborane isomer (*ortho* > *meta* > *para*), suggesting that the electron-withdrawing carborane cage is influencing the HOMO to a greater extent than the LUMO, such that the band gap is increased for the most electron-withdrawing isomer. Similarly, the fact that the *trans* isomers are more blue-shifted than the *cis* isomers would imply that the *trans* isomers are better able to conjugate with the backbone, more effectively withdrawing electron density than the *cis* isomers. This may be expected for steric reasons. Additionally, a long wavelength shoulder is observed in all spectra, the intensity of which decreased with increasing solution temperature, indicative of some degree of aggregation, even in dilute solution. No apparent trend was seen in the degrees of aggregation observed: in the *cis* polymers the intensity was greatest in *ortho* > *meta* > *para*, with the reverse true upon switching to the *trans* isomer. The concentrations of all solutions were comparable, confirming that these observations are a result of polymer structure rather than simply dilution.

Upon moving to thin film, a red-shift in the absorbance spectra of all six polymers was observed, implying the presence of some degree of ordering in the solid state (Fig. 3). In addition a clear shoulder around 600 nm was observed for all polymer films. No notable changes were observed following thermal annealing at 160 °C, implying that the as-cast morphologies were not significantly changed by thermal treatment

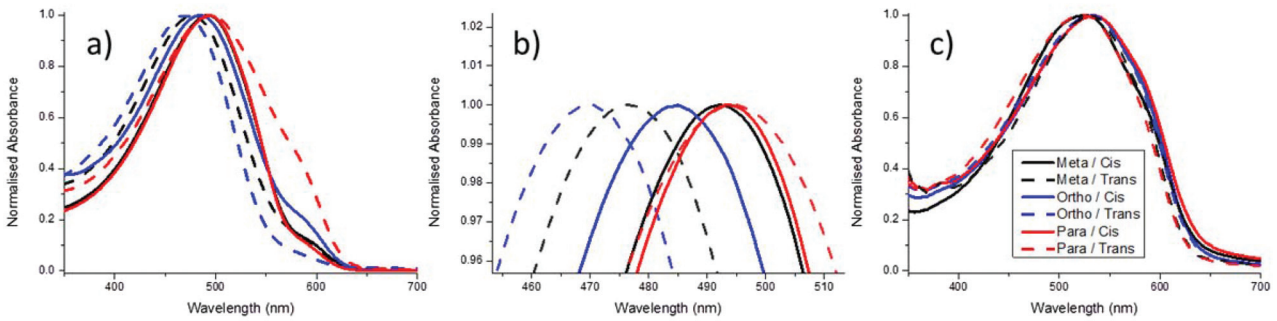

Fig. 3 Peak normalised UV-Vis absorption spectra of the polymers in (a) dilute chlorobenzene solution (b) a close-up of the solution λ_{max} region (c) as spun cast thin films.

Table 3 Energetic properties

Polymer	HOMO[a] (eV)	LUMO[b] (eV)	E_g[c] (eV)
ortho/*cis*	−5.88	−3.92	1.96
ortho/*trans*	−5.89	−3.92	1.97
meta/*cis*	−5.41	−3.44	1.97
meta/*trans*	−5.44	−3.45	1.99
para/*cis*	−5.48	−3.52	1.96
para/*trans*	−5.24	−3.25	1.99

[a] Measured as a thin film by PESA (error ±0.05 eV). [b] Estimated by subtracting the optical band gap from the measured ionisation potential. [c] Determined from absorption onset in solid state.

and agreeing with observations made by Huang *et al.* on polythiophenes with bulky pendant groups.[12] All polymers exhibited a comparable λ_{max}, suggesting that solid-state organisation is largely independent of the pendant group regiochemistry.

Energetic properties

Polymeric ionisation potentials were measured by PESA analysis of spin-coated films. In both the *cis* and *trans* derivatives, the ionisation potentials of the *ortho*-carborane containing polymers was significantly greater than the *meta* and *para* equivalents (Table 3). This supports observations made in the UV-Vis analysis, that the *ortho*-carborane polymers had a larger electron withdrawing effect on the conjugated backbone. The trend for *meta* and *para* isomers is less clear, with similar values observed for all isomers except *para*/*trans*, which appears anomalous. This may be due to the difficulties in forming a homogeneous film of this polymer, which exhibited the lowest solubility.

The optimised structures of all six polymers were predicted by DFT calculations, performed using Gaussian09 with the B3LYP/6-31G* basis set.[39] In all cases only regioregular head-to-tail sidechains were considered, although in reality it is likely that head-to-head and tail-to-tail linkages were also present. In the case of head-to-tail linkages, it was apparent that for all isomers the presence of the vinyl-carborane moiety induced a slight out-of-plane twist along the polymer backbone (Fig. 4 and Fig. S13–S16†). However, upon visualisation of the molecular orbitals (Fig. 5 and ESI S17–S20†) it was observed that this twist did not significantly impair electronic delocalisation along the thiophene backbone. Additionally, the models suggest that the out-of-plane displacements are greater in the *cis* isomers than their *trans* counterparts, likely due to the closer proximity of the carborane cage to the thiophene backbone in the *cis* polymers.

Visualisation of the frontier molecular orbitals suggested that neither the HOMO nor LUMO, despite their homogeneous distribution along the polymer backbone, significantly extended onto the pendant carborane groups, although there is some delocalisation onto the vinylene groups. This is quite different to results of Zhang and co-workers, who reported localisation of the LUMO wavefunction on the side chain rather than the backbone when an electron-withdrawing cyano

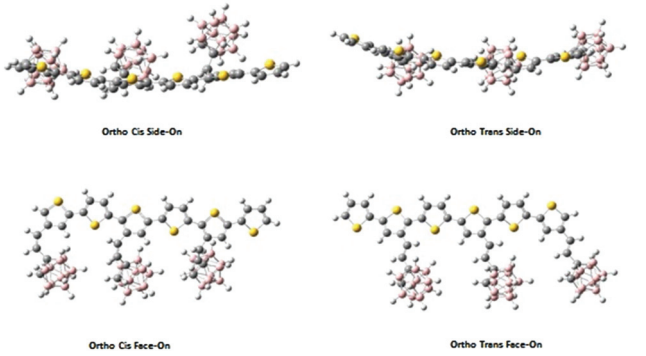

Fig. 4 Energy minimised structures of *ortho*/*cis* and *ortho*/*trans* polymers. Calculated in Gaussian09 with the B3LYP/6-31G* basis set.

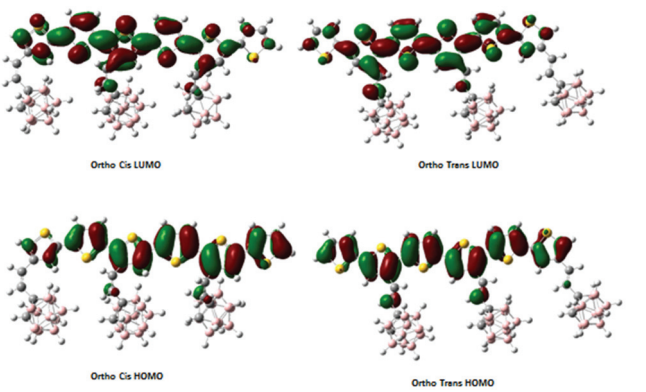

Fig. 5 Visualised frontier molecular orbitals of *ortho*/*cis* and *ortho*/*trans* polymers. Calculated in Gaussian09 with the B3LYP/6-31G* basis set.

containing pendant groups were incorporated onto the polymer.[40] In the present case the main effect of carborane seems to be inductive electron withdrawal, corroborating results on other reported carborane containing conjugated polymers.[25,26]

DFT-predicted HOMO and LUMO values show a similar trend as those determined experimentally, with the *ortho*-carborane containing polymers exhibiting lower HOMO and LUMO levels than those containing the *meta* and *para* isomers (Table 4). DFT calculations also predict a difference in frontier orbital energies between the *cis* and *trans* isomers, which we do not observe experimentally. This may be due to the differences in regioregularity between the modelled oligomers and

Table 4 DFT-predicted energetic properties

Polymer	HOMO (eV)	LUMO (eV)	E_g (eV)
ortho/*cis*	−5.10	−2.67	2.43
ortho/*trans*	−5.41	−2.65	2.75
meta/*cis*	−4.95	−2.50	2.45
meta/*trans*	−5.17	−2.39	2.78
para/*cis*	−4.97	−2.52	2.44
para/*trans*	−5.15	−2.37	2.78

the actual polymers, in which the sidechains are not expected to the regioregular.

Physical properties

The solid state morphology of the polymers was investigated by XRD spectroscopy, analysing drop-cast films both as cast and following annealing at 160 °C for five minutes (Fig. 6). A weak and broad first order lamellar (d_{100}) reflection was observed in all *trans*-vinylene polymers, whereas in the *cis* polymers a comparable reflection was observed only in the presence of *ortho*-carborane. Polymer ordering was largely unchanged following thermal treatment, with the low intensity reflection peaks indicating a high degree of amorphous character for all polymers, potentially arising from the twisted backbone and non-planar pendant groups, as well as the regiorandom nature of the sidechains. These results are comparable to those reported by Zou and co-workers, who observed high amorphous character when phenothiazine was employed as a pendant group, suggesting that polymer morphology is sidechain dependent.[17,41] In all instances DSC analysis showed no obvious thermal transitions between 0 °C and 300 °C at a heating rate of 10 °C min^{-1}. Taken together with the UV data these results suggest that although the polymers have a tendency to aggregate, there is little long range order in these aggregates. The thermal stability of all six polymers was good, with 5% mass loss temperatures ranging from 330 °C to 400 °C (see ESI S21–S23†).

Charge transport properties

Top gate, bottom contact (TGBC) organic field effect transistors were prepared using pentafluorobenzenethiol treated gold electrodes and an amorphous fluoropolymer dielectric layer. For each device the polymer was spun-cast from chlorobenzene solution before heating at 160 °C to ensure any residual solvent was evaporated before completion of the device. The OFET characteristics of all six polymers are summarised in Table 5 (see ESI S24–S29† for OFET transfer and output curves).

Table 5 Summary of TG,BC OFET characteristics showing saturated mobility, threshold voltage and on/off ratio

Polymer	μ_{sat} ($cm^2\ V^{-1}\ s^{-1}$)	V_T (V)	I_{on}/I_{off}
ortho/cis	9.6×10^{-5}	66	~10
ortho/trans	1.3×10^{-4}	90	~10
meta/cis	3.7×10^{-4}	50	$\sim 10^2$
meta/trans	5.5×10^{-5}	96	~10
para/cis	1.4×10^{-4}	32	$\sim 10^2$
para/trans	1.3×10^{-4}	37	~10

In general, the transistor performance of all polymers was relatively low, with charge carrier mobilities similar to those exhibited by regiorandom P3HT.[42] In particular, the poor film-forming abilities of the *trans* polymers led to difficulties in device fabrication, with the devices showing high gate leakage, which may result in an overestimation of the charge carrier mobility if not taken into consideration. In all instances, the device threshold voltages were rather large, and there were clear issues with charge injection, particularly for the *ortho* polymers (see output plots S24–S25†) which we attribute to the high ionisation potentials of the polymers (Table 3). The rather low mobilities of all six polymers can be explained by the largely amorphous film morphology, as well as the non-planarity of the conjugated backbones reducing π–π stacking interactions between adjacent chains and impeding the long range order necessary for charge transport.

Photovoltaic properties

OPV devices were prepared with a conventional device structure consisting of ITO/PEDOT-PSS/polymer/PCBM/Ca/Al and tested under simulated AM1.5 illumination. Films were spun from a 1 : 2 wt% (polymer : $PC_{70}BM$) chlorobenzene solution and had comparable thickness in all cases. *J*–*V* curves of the polymers are shown in Fig. 7 with the corresponding open-circuit voltages (V_{OC}), short-circuit currents (J_{SC}), fill factors (FF) and power conversion efficiencies (PCE) shown in Table 6.

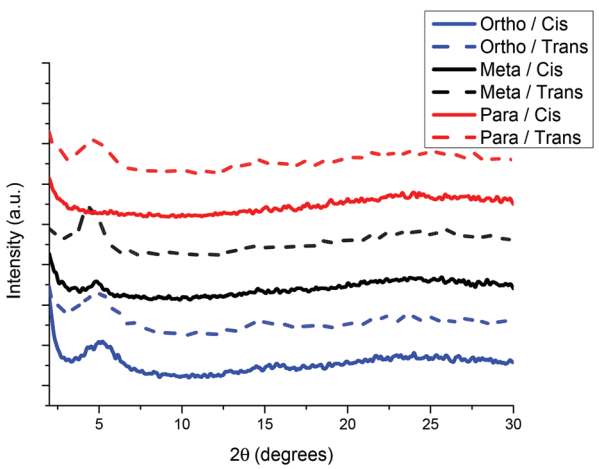

Fig. 6 XRD spectra of polymer films following annealing at 160 °C for five minutes. Offset for clarity.

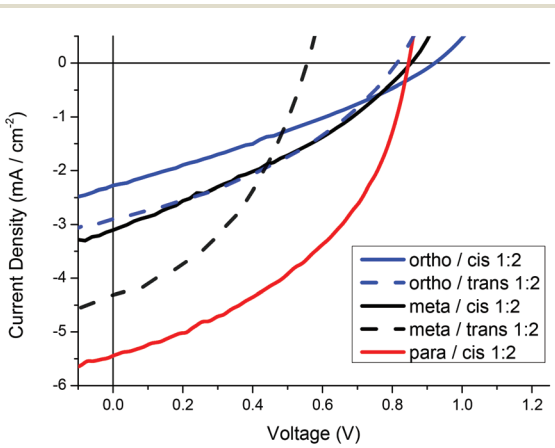

Fig. 7 *J*–*V* curves of OPV devices with active layer produced from 1 : 2 wt% polymer : PC70BM blend ratio.

Table 6 Summary of OPV characteristics

Polymer	V_{OC} (V)	J_{SC} (mA cm^{-2})	Fill factor	PCE[a] (%)
ortho/*cis*	0.92	2.28	0.30	0.63 (0.59, 5)
ortho/*trans*	0.82	2.92	0.37	0.88 (0.86, 3)
meta/*cis*	0.85	3.11	0.32	0.86 (0.80, 3)
meta/*trans*	0.56	4.34	0.42	1.01 (0.95, 4)
para/*cis*	0.85	5.44	0.44	2.03 (1.90, 4)
para/*trans*	—	—	—	—

[a] Highest performing device reported. Average device performance and sample size shown in parentheses.

Unfortunately no devices could be produced from the *para*/*trans* polymer due to poor solubility, which led to problems with film formation.

The device performance of all five polymers was relatively low, mainly due to a combination of low fill factors and photocurrents, although voltages were respectable. In common with other largely amorphous donor polymers, relatively high loadings of PCBM were required to ensure reasonable performance, which can be related to the requirement to drive phase segregation in the film.[43] The overall low performance can probably be related to the low degree of structural order and low charge carrier mobilities, but nevertheless, differences between isomers can be observed. Comparing the *cis* polymer series, a slightly larger V_{OC} was observed for *ortho*-carborane containing polymers, over the *meta* and *para*, in agreement with the trend in ionisation potentials. Although a larger open-circuit voltage might have been expected for the *ortho* polymer simply on the basis of ionisation potentials, the fact this was not observed is likely due to the far from ideal device characteristics, with high degrees of charge recombination likely. Photocurrent and fill factor increased from *ortho* < *meta* < *para* carborane, such that the *para*/*cis* polymer had the best overall device PCE of 2%. As far as we are aware this is the best efficiency so far reported for any carborane containing polymer. In the *trans* series, the same relative trend is seen as for the *cis*, *i.e.* the *ortho* polymer has a higher voltage but lower photocurrent and fill factor when compared to the *meta* polymer. Finally, it is also possible to compare between the *ortho* and *meta* substituted polymers for both *trans* and *cis* derivatives. In both cases we observed that the *trans* polymers have higher overall efficiency, due to higher fill factors and photocurrent, but lower voltages. Such improvements could be related to the reduction in backbone twisting for the *trans* isomer *versus* the *cis*.

Conclusions

We report the synthesis of a novel series of soluble thiophene moieties with carborane pendant groups. All three (*ortho*, *meta* and *para*) isomers of carborane were employed *via cis* and *trans* vinylene linker groups. The novel monomers were incorporated into semiconducting polymers whose solution-state optical properties and crystallinities were shown to be determined by pendant group stereochemistries. Analysis of OPV devices showed that the presence of *ortho*-carborane led to an increase in V_{OC} whereas *para*-carborane enabled J_{SC} to be maximised. The highest performing device offered a PCE of 2.03%, despite exhibiting a low fill factor of only 0.41. Further optimisation of this class of material, for example by the synthesis of regioregular polymers – which might exhibit improved solid state ordering – may offer an opportunity to further improve performance.

Acknowledgements

We thank AWE for financial support of an EPSRC CASE award (EP/1501444/1) and for their input and support of this project.

Notes and references

1 M. T. Dang, L. Hirsch and G. Wantz, *Adv. Mater.*, 2011, **23**, 3597–3602.
2 M. T. Dang, L. Hirsch, G. Wantz and J. D. Wuest, *Chem. Rev.*, 2013, **113**, 3734–3765.
3 F. P. V. Koch, J. Rivnay, S. Foster, C. Müller, J. M. Downing, E. Buchaca-Domingo, P. Westacott, L. Yu, M. Yuan, M. Baklar, Z. Fei, C. Luscombe, M. A. McLachlan, M. Heeney, G. Rumbles, C. Silva, A. Salleo, J. Nelson, P. Smith and N. Stingelin, *Prog. Polym. Sci.*, 2013, **38**, 1978–1989.
4 S. Holliday, J. E. Donaghey and I. McCulloch, *Chem. Mater.*, 2014, **26**, 647–663.
5 X. Guo, M. Baumgarten and K. Müllen, *Prog. Polym. Sci.*, 2013, **38**, 1832–1908.
6 S. Allard, M. Forster, B. Souharce, H. Thiem and U. Scherf, *Angew. Chem., Int. Ed.*, 2008, **47**, 4070–4098.
7 F. C. Krebs, *Org. Electron.*, 2009, **10**, 761–768.
8 I. McCulloch, R. S. Ashraf, L. Biniek, H. Bronstein, C. Combe, J. E. Donaghey, D. I. James, C. B. Nielsen, B. C. Schroeder and W. Zhang, *Acc. Chem. Res.*, 2012, **45**, 714–722.
9 J. Mei and Z. Bao, *Chem. Mater.*, 2014, **26**, 604–615.
10 T. Lei, J.-Y. Wang and J. Pei, *Chem. Mater.*, 2014, **26**, 594–603.
11 J.-H. Tsai, W.-Y. Lee, W.-C. Chen, C.-Y. Yu, G.-W. Hwang and C. Ting, *Chem. Mater.*, 2010, **22**, 3290–3299.
12 Y. Huang, Y. Wang, G. Sang, E. Zhou, L. Huo, Y. Liu and Y. Li, *J. Phys. Chem. B*, 2008, **112**, 13476–13482.
13 Y. Li, *Acc. Chem. Res.*, 2012, **45**, 723–733.
14 H.-J. Wang, J.-Y. Tzeng, C.-W. Chou, C.-Y. Huang, R.-H. Lee and R.-J. Jeng, *Polym. Chem.*, 2013, **4**, 506.
15 J. Hou, C. Yang, C. He and Y. Li, *Chem. Commun.*, 2006, 871–873.
16 P. Shen, H. Bin, L. Xiao and Y. Li, *Macromolecules*, 2013, **46**, 9575–9586.
17 Y. Zou, W. Wu, G. Sang, Y. Yang and Y. Liu, *Macromolecules*, 2007, 7231–7237.

18 R. N. Grimes, *Carboranes*, Academic Press, New York, 2nd edn, 2011.
19 E. Hao, B. Fabre, F. R. Fronczek and M. G. H. Vicente, *Chem. Commun.*, 2007, 4387–4389.
20 K. Kokado and Y. Chujo, *Macromolecules*, 2009, **42**, 1418–1420.
21 K. Kokado, Y. Tokoro and Y. Chujo, *Macromolecules*, 2009, **42**, 2925–2930.
22 M. H. Park, K. M. Lee, T. Kim, Y. Do and M. H. Lee, *Chem. – Asian. J.*, 2011, **6**, 1362–1366.
23 B. Fabre, S. Chayer and M. G. H. Vicente, *Electrochem. Commun.*, 2003, **5**, 431–434.
24 J. J. Peterson, A. R. Davis, M. Werre, E. B. Coughlin and K. R. Carter, *ACS Appl. Mater. Interfaces*, 2011, **3**, 1796–1799.
25 J. Marshall, Z. Fei, C. P. Yau, N. Yaacobi-Gross, S. Rossbauer, T. D. Anthopoulos, S. E. Watkins, P. Beavis and M. Heeney, *J. Mater. Chem. C*, 2014, **2**, 232–239.
26 J. Marshall, B. C. Schroeder, H. Bronstein, I. Meager, S. Rossbauer, N. Yaacobi-Gross, E. Buchaca-Domingo, T. D. Anthopoulos, N. Stingelin, P. Beavis and M. Heeney, *Macromolecules*, 2014, **47**, 89–96.
27 K. Kokado, Y. Tokoro and Y. Chujo, *Macromolecules*, 2009, **42**, 9238–9242.
28 J. J. Peterson, Y. C. Simon, E. B. Coughlin and K. R. Carter, *Chem. Commun.*, 2009, 4950–4952.
29 A. R. Davis, J. J. Peterson and K. R. Carter, *ACS Macro Lett.*, 2012, **1**, 469–472.
30 Y. Morisaki, M. Tominaga, T. Ochiai and Y. Chujo, *Chem. – Asian J.*, 2014, **9**, 1247–1251.
31 Y. C. Simon, J. J. Peterson, C. Mangold, K. R. Carter and E. B. Coughlin, *Macromolecules*, 2009, **42**, 512–516.
32 Y. Li, H.-Q. Wu, H.-L. Xu, S.-L. Sun and Z.-M. Su, *J. Mol. Model*, 2013, **19**, 3741–3747.
33 P. Dozzo, R. A. Kasar and S. B. Kahl, *Inorg. Chem.*, 2005, **44**, 8053–8057.
34 A. Sousa-Pedrares, C. Viñas and F. Teixidor, *Chem. Commun.*, 2010, **46**, 2998–3000.
35 S. Tierney, M. Heeney and I. McCulloch, *Synth. Met.*, 2005, **148**, 195–198.
36 K. T. Nielsen, H. Spanggaard and F. C. Krebs, *Macromolecules*, 2005, **38**, 1180–1189.
37 R. S. Loewe and R. D. McCullough, *Chem. Mater.*, 2000, **12**, 3214–3221.
38 M. Al-Hashimi, M. A. Baklar, F. Colleaux, S. E. Watkins, T. D. Anthopoulos, N. Stingelin and M. Heeney, *Macromolecules*, 2011, **44**, 5194–5199.
39 G. Frisch, *et al.*, *Gaussian 09 Version B.01*, Gaussian, Inc., Wallingford, CT, 2009.
40 Z.-G. Zhang, Y.-L. Liu, Y. Yang, K. Hou, B. Peng, G. Zhao, M. Zhang, X. Guo, E.-T. Kang and Y. Li, *Macromolecules*, 2010, **43**, 9376–9383.
41 G. Sang, Y. Zou and Y. Li, *J. Phys. Chem. C*, 2008, **112**, 12058–12064.
42 H. Sirringhaus, P. J. Brown, R. H. Friend, M. M. Nielsen, K. Bechgaard and A. J. H. Spiering, *Nature*, 1999, **401**, 685–688.
43 C. J. Brabec, M. Heeney, I. McCulluch and J. Nelson, *Chem. Soc. Rev.*, 2011, **40**, 1185–1199.